2. R. R. Ernst, G. Bodenhausen, A. Wokaun, *Principles of Nuclear Magnetic Resonance in One and Two Dimensions* (Oxford Univ. Press, Oxford, 1990).
3. K. Wüthrich, *NMR of Proteins and Nucleic Acids* (Wiley, New York, 1986).
4. R. G. Griffin *et al.*, in *Physics of NMR Spectroscopy in Biology and Medicine*, B. Maraviglia, Ed. (North-Holland, New York, 1988), pp. 203–266.
5. E. R. Andrew, A. Bradbury, R. G. Eades, *Nature* **182**, 1659 (1958).
6. I. J. Lowe, *Phys. Rev. Lett.* **2**, 285 (1959).
7. A. Pines, M. G. Gibby, J. S. Waugh, *J. Chem. Phys.* **59**, 569 (1973).
8. J. Schaefer and E. O. Stejskal, *J. Am. Chem. Soc.* **98**, 1031 (1976).
9. E. R. Andrew, S. Clough, L. F. Farnell, T. D. Gledhill, I. Roberts, *Phys. Lett.* **21**, 505 (1966).
10. E. R. Andrew, A. Bradbury, R. G. Eades, V. T. Wynn, *ibid.* **4**, 99 (1963).
11. D. P. Raleigh, M. H. Levitt, R. G. Griffin, *Chem. Phys. Lett.* **146**, 71 (1988).
12. D. P. Raleigh, F. Creuzet, S. K. Das Gupta, M. H. Levitt, R. G. Griffin, *J. Am. Chem. Soc.* **111**, 4502 (1989).
13. A. E. McDermott *et al.*, *Biochemistry* **29**, 5767 (1990).
14. M. G. Columbo, B. H. Meier, R. R. Ernst, *Chem. Phys. Lett.* **146**, 189 (1988).
15. E. W. J. R. Maas and W. S. Veeman, *ibid.* **149**, 170 (1988).
16. F. Creuzet, D. P. Raleigh, M. H. Levitt, R. G. Griffin, unpublished results.
17. M. H. Levitt, D. P. Raleigh, F. Creuzet, R. G. Griffin, *J. Chem. Phys.* **92**, 6347 (1990).
18. Z. Gan and D. M. Grant, *Mol. Phys.* **67**, 1419 (1990).
19. W. J. DeGrip, *Photochem. Photobiol.* **48**, 799 (1988).
20. R. A. Mathies, S. O. Smith, I. Palings, in *Biological Applications of Raman Spectroscopy*, T. Spiro, Ed. (Wiley, New York, 1987), pp. 59–108.
21. B. Honig, A. D. Greenburg, U. Dinur, T. G. Ebrey, *Biochemistry* **15**, 4593 (1976).
22. B. Honig, B. Hudson, B. D. Sykes, M. Karplus, *Proc. Natl. Acad. Sci. U.S.A.* **68**, 1289 (1971).
23. G. S. Harbison *et al.*, *Biochemistry* **24**, 6955 (1985).
24. G. S. Harbison *et al.*, *J. Am. Chem. Soc.* **107**, 4809 (1985).
25. H. Rodman-Gilson and B. Honig, *ibid.* **110**, 1943 (1988).
26. C. H. Stam and C. H. MacGillavry, *Acta Cryst. allogr.* **16**, 62 (1963).
27. C. H. Stam, *Acta Crystallogr. Sect. B* **28**, 2936 (1972).
28. This procedure differed from that used previously, in that here the centerband intensity was used, while in our previous analysis of Zn acetate and tyrosine ethyl ester the sum of the integrated centerband and sidebands was used. The major reason for this change in analysis was to improve the signal-to-noise ratio in the intensity measurement, since the signal-to-noise ratio for bR is such that the sidebands and the wings of the centerband cannot be measured accurately. We find that analysis of zinc acetate and retinoic acid data by this method (see below) results in good agreement with crystallographic distances. Furthermore, for the $n = 1$ resonance used here, the spinning speeds are large compared to $\Delta\sigma$ and therefore the sideband intensities, and the errors generated by ignoring them, are small.
29. J. Herzfeld and A. E. Berger, *J. Chem. Phys.* **73**, 6021 (1980).
30. A. Kubo and C. A. McDowell, *J. Chem. Soc. Faraday Trans.* **C84**, 3713 (1988).
31. E. K. Wolff, R. G. Griffin, J. S. Waugh, *J. Chem. Phys.* **67**, 2387 (1977).
32. M. Mehring, *Principles of High-Resolution NMR in Solids* (Springer-Verlag, Berlin, 1983), pp. 250–257.
33. Supported by the National Institutes of Health (GM-23403, GM-36810, GM-36920, and RR-00995), and by the Netherlands Foundation for Chemical Research and the Netherlands Organization for the Advancement of Scientific Research. F. C. was supported by a Bantrell Fellowship and A. M. by an American Cancer Society Postdoctoral Fellowship (PF-3283).

27 August 1990; accepted 9 November 1990

Baddeleyite-Type High-Pressure Phase of TiO_2

H. Sato, S. Endo,* M. Sugiyama, T. Kikegawa, O. Shimomura, K. Kusaba

A high-pressure phase of TiO_2, which had been observed by shock-wave experiments and remained unresolved, has been studied by in situ x-ray diffraction. The single phase was formed at 20 gigapascals and 770°C with the use of sintered-diamond multianvils; it has the same structure as baddeleyite, the stable phase of ZrO_2 at ambient conditions. The coordination number of Ti increases from six to seven across the rutile to baddeleyite transition, and the volume is reduced by approximately 9 percent.

STUDY OF PRESSURE-INDUCED PHASE transitions of dioxides provides an understanding of crystal structure and bonding and mineral stability in planets. The TiO_2 system provides an analog to the SiO_2 system; for example, stishovite (a high-pressure form of SiO_2) has a rutile structure. Many workers have investigated phase relations in the TiO_2 system (*1*). On the basis of shock-wave experiments, McQueen *et al.* (*2*) reported that TiO_2 underwent a phase transition beginning at 33 GPa and terminating at 100 GPa, accompanied by ~20% volume reduction. They found that the sample after compression to 75 GPa was a mixture of rutile and α-PbO_2 (columbite)–type structures. Mashimo *et al.* (*3*) observed a strong dependence of the onset pressure of the transition on the shock propagation direction. The transition began at 12.2, 17.0, or 33.7 GPa along the [100], [110], or [001] axis, respectively. These results were confirmed by Syono *et al.* (*4*), who reported, in addition, that this transition terminates at ~70 GPa and that another transition takes place around 100 PGa. These two transitions were not separately observed by either McQueen *et al.* (*2*) or Al'tshuler *et al.* (*5*).

The determination of the crystal structure of the phase beginning to appear at 12 to 34 GPa has been a problem for a quarter of a century. The α-PbO_2 phase in the sample recovered after compression beyond the transition pressure cannot be a candidate, because its volume is only ~2% smaller than that of rutile (*2*); the α-PbO_2 phase has been assumed to be a metastable modification of the high-pressure phase, which might have a structure such as that of fluorite. X-ray studies at room temperature have shown that no apparent phase transition occurs up to 18 GPa (*2*). However, in studies with a diamond-anvil cell and a laser heating technique, two different high-pressure phases were reported (*6, 7*); one was a hexagonal phase with volume smaller by 10.5% than that of rutile at 25 GPa and room temperature after heating up to ~1000°C (*6*), and the other was an orthorhombic phase at 20 GPa after almost the same heat treatment (*7*). In this report we describe the in situ x-ray determination of the crystal structure of this high-pressure phase.

High pressure and high temperature were generated with so-called 6–8 type double-stage multianvils; sintered-diamond was used for the second-stage eight anvils (*8*). The synchrotron radiation used for the structure

Table 1. Observed (obs) and calculated (calc) x-ray diffraction data of TiO_2 at 20.3 GPa and room temperature. The sample was heated at 770°C for 30 min and then quenched to room temperature while at 20.3 GPa. Monoclinic cell parameters were determined to be $a = 4.64 \pm 0.01$ Å, $b = 4.76 \pm 0.01$ Å, $c = 4.81 \pm 0.01$ Å, $\beta = 99.2 \pm 0.4°$, $Z = 4$, and $V = 104.8 \pm 0.5$ A^3 by the least-square method.

d_{obs} (Å)	Baddeleyite type			
	d_{calc} (Å)	*h*	*k*	*l*
3.37	3.36	0	1	1
3.32	3.30	1	1	0
2.858	2.869	1	1	$\bar{1}$
2.588	2.574	1	1	1
2.357	2.378	0	2	0
	2.376	0	0	2
2.281	2.289	2	0	0
1.987	2.000	2	1	$\bar{1}$
	1.984	1	2	$\bar{1}$
	1.982	1	0	2
1.834	1.830	1	1	2
1.803	1.799	2	0	$\bar{2}$
1.691	1.681	0	2	2
1.660	1.649	2	2	0
	1.639	1	2	$\bar{2}$
1.629	1.617	2	2	$\bar{1}$
1.532	1.526	3	0	0
1.494	1.503	0	1	3
	1.498	1	3	0
	1.497	1	1	$\bar{3}$
1.440	1.453	3	1	$\bar{1}$
	1.451	1	3	$\bar{1}$
	1.435	2	2	$\bar{2}$

H. Sato, S. Endo, M. Sugiyama, Research Center for Extreme Materials, Osaka University, Toyonaka, Osaka 560, Japan.
T. Kikegawa, National Laboratory for High Energy Physics, Tsukuba 305, Japan.
O. Shimomura, National Institute for Research in Inorganic Materials, Tsukuba 305, Japan.
K. Kusaba, Institute for Materials Research, Tohoku University, Sendai 980, Japan.

*To whom correspondence should be addressed.

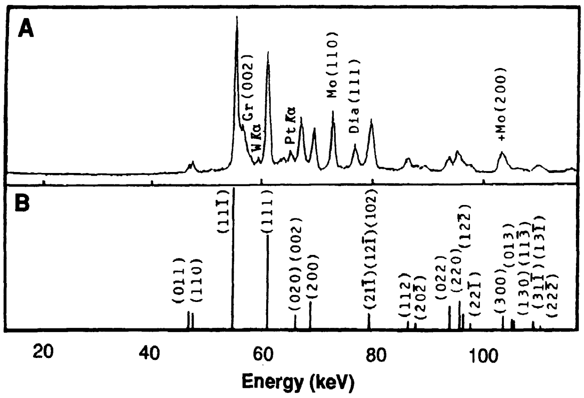

Fig. 1 (**A**) X-ray diffraction pattern of TiO_2 at 20.3 GPa and room temperature after heating at 770°C ($2\theta = 4.5°$). The diffraction lines of the materials constituting the cell (the graphite heater and molybdenum electrode) and the sintered diamond anvils also appear in the pattern. (**B**) Diffraction lines with calculated *d*-values for the monoclinic baddeleyite-type structure listed in Table 1 and with the same intensities as baddeleyite (ZrO_2) (*16*).

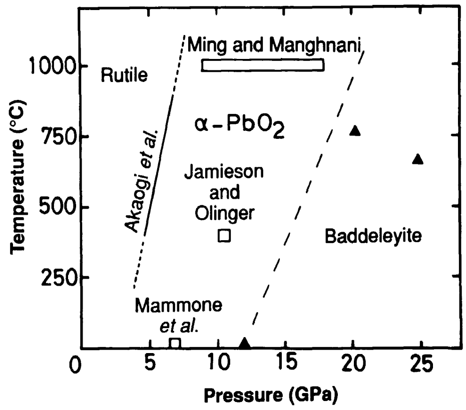

Fig. 3. Hypothetical phase diagram of TiO_2. The rutile-α-PbO_2 boundary is from (*14*), and the stability range of α-PbO_2 phase is inferred from data in (*7*), (*12*), and (*13*). Triangles represent our data on the formation of the baddeleyite phase.

determination was sufficiently intense for a diffracted beam to pass through the sintered diamond anvil containing Co metal as a binder. Analysis was by energy-dispersive diffractometry. The starting material was a powder sample obtained by grinding a single crystal of rutile with 99.99% purity (synthesized at Nakazumi Crystal Laboratory).

In a room-temperature experiment, some diffraction lines in addition to the x-ray pattern of rutile began to appear at $\sim$12 GPa, and the intensities of these new lines became greater than those of the remaining rutile lines at 20 GPa. The sample released from pressure was a mixture of rutile and α-PbO_2 phase. In another run, the sample was heated at 770°C for 15 min at 20.3 GPa. The lines of the rutile phase disappeared completely, and only the new lines were observed. Some of the broad new lines observed in the room-temperature experiment became two or three sharp lines, with heating. The pattern of the sample at 20.3 GPa after cooling to room temperature (Fig. 1A) was almost the same as that at 770°C. We increased the pressure of the sample to 25 GPa and heated it again to 670°C, but observed no appreciable change in the x-ray pattern. The pattern of the sample brought back to ambient conditions was identified as α-PbO_2 phase and a small amount of rutile.

The pattern of Fig. 1A was used to determine the crystal structure. In this pattern there is no single (111) diffraction line characteristic of the fluorite structure, which might be expected as a post-rutile phase. Instead, there are two lines, which are assumed to be the (111) and (11$\bar{1}$) lines of a monoclinic lattice. The pattern of the high-pressure phase is most similar to that of baddeleyite (space group $P2_1/c$), the stable phase of ZrO_2 at ambient conditions (Table 1 and Fig. 1B). The uniform pressure and temperature generated with the multianvil system enabled the formation of a single phase, and the large sample volume (1.0 mm in diameter and 0.6 mm in thickness) contributed to the quality of x-ray patterns. Although the present pattern resembles closely the one obtained by Ming and Manghnani (*7*) using a diamond cell, they did not observe the two weak (011) and (110) lines in the low-energy region (Fig. 1), and this resulted in the incorrect determination of the crystal structure. The pattern by Liu (*6*) is significantly different from ours at 20 GPa and 25 GPa.

The volume reduction accompanying the transition from the rutile to the baddeleyite phase at 20.3 GPa is about 9% (Fig. 2) on the basis of available data on rutile (*4, 9, 10*). This value at the transition could not be determined definitely in the shock-wave experiments, in which the transition extended over a wide pressure range.

Many investigators have supposed that the high-pressure phase of TiO_2 has a fluorite structure, in which a Ti atom is coordinated by eight O atoms. Our data, however, clarify that it has the structure of baddeleyite. Baddeleyite is considered as one of the distorted fluorite structures, and in it, the Ti atoms are coordinated by seven O atoms (*11*). At ambient conditions, HfO_2 also has this structure; thus, the dioxide of Ti under pressure takes the ambient-pressure structure of the dioxides of Zr and Hf, which are in the same group as Ti (IVA) but have larger ionic radii.

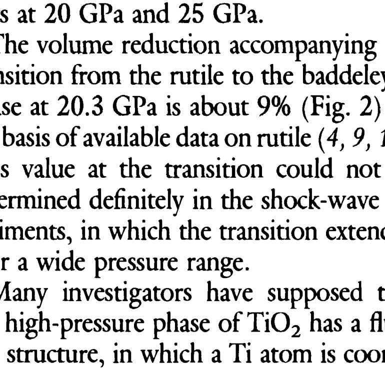

Fig. 2. Molar volumes of the rutile (●) and baddeleyite (▲) phases of TiO_2 as a function of pressure at room temperature. X-ray data by Sato (*9*) (○) and Ming and Manghnani (⊗) (*10*) for the rutile phase are shown; their highest pressure data only are shown, and molar volume was calculated from the relative volume change. Hugonio data by Syono *et al.* (*4*) are represented by the dashed line. The volume of α-PbO_2 phase in the pressure-released sample is shown by the solid square.

Jamieson and Olinger (*12*) observed the transition from rutile to the α-PbO_2 phase at 10.6 GPa and 400°C. On the basis of Raman study, Mammone *et al.* (*13*) reported that a small amount (10 to 20%) of α-PbO_2 phase was formed from rutile at about 7 GPa and room temperature. Ming and Manghnani (*7*) also observed this transition at $\sim$1000°C at a pressure between 9 and 18 GPa. If the α-PbO_2 phase is stable in a limited pressure-temperature range, as these results indicate, the following sequence of phases is likely as pressure increases: rutile → α-PbO_2 type → baddeleyite type. A hypothetical phase diagram of TiO_2 is shown in Fig. 3. The boundary between the rutile and α-PbO_2 phases is based on the experimental result by Akaogi *et al.* (*14*). The boundary between the α-PbO_2 and baddeleyite phases is tentatively drawn as passing through the point 12 GPa and 25°C, at which we observed the onset of the formation of the baddeleyite phase. However, the observation that rutile directly transformed to the baddeleyite phase seems to contradict the relations shown in the hypothetical diagram. We attribute this observation to the extreme sluggishness of the rutile → α-PbO_2 phase transition at room temperature. Akaogi *et al.* (*14*) and Mammone *et al.* (*13*) reported that this transition occurred slowly below 800°C. The presence of the α-PbO_2 phase in the samples recovered from 20 and 25 GPa indicates that the baddeleyite phase was transformed back to the α-PbO_2 phase on decompression but that the α-PbO_2 phase was scarcely transformed back to rutile. The reverse transition, α-PbO_2 → rutile, must be sluggish, too.

This notion is consistent with the description by McQueen *et al.* (*2*), that the metastable α-PbO_2 phase at ambient conditions was transformed back to rutile by heating at 400°C. The rutile → α-PbO_2 type transition may be a reconstructive-type transition with large atomic displacement (*15*).

Thus, our work indicates that the first transition observed by Syono *et al.* (*4*) corresponds to the formation of the baddeleyite phase and that the second transition, around 100 GPa, may correspond to the pressure-induced transition already observed in ZrO_2.

REFERENCES AND NOTES

1. See, for example, L. Liu and W. A. Bassett, *Elements, Oxides, and Silicates* (Oxford Univ. Press and Clarendon Press, New York and Oxford, 1982), pp. 92–195.
2. R. G. McQueen *et al.*, *Science* **155**, 1401 (1967).
3. T. Mashimo, K. Nagayama, A. Sawaoka, *J. Appl. Phys.* **54**, 5043 (1983).
4. Y. Syono, K. Kusaba, M. Kikuchi, K. Fukuoka, T. Goto, in *High-Pressure Research in Mineral Physics*, M. H. Manghnani and Y. Syono, Eds. (Terra Scientific, Tokyo, 1987), pp. 385–392.
5. L. V. Al'tshuler, M. A. Podurets, G. V. Simakov, R. F. Trunin, *Sov. Phys. Solid State* **15**, 969 (1973).
6. L. Liu, *Science* **199**, 422 (1978).
7. L. C. Ming and M. H. Manghnani, *High-Pressure Research in Geophysics*, S. Akimoto and M. H. Manghnani, Eds. (Center for Academic Publications Japan/Tokyo and Reidel/Dordrecht, 1982), pp. 329–347.
8. The method is almost the same as that adopted for the observation of the high-pressure transitions in SnO_2 by S. Endo *et al.* [*High Press. Res.* **4**, 408 (1990)]. The cubic press, MAX80, at the National Laboratory for High Energy Physics was mainly used. A boron-epoxy cell was used as a pressure medium, and the pressure was calibrated on the basis of the compression of NaCl and Au at room temperature. High temperature was generated by a graphite heater inserted in a cell and measured by a Pt-Pt13Rh thermocouple.
9. Y. Sato, in *High-Pressure Research: Applications in Geophysics*, M. H. Manghnani and S. Akimoto, Eds. (Academic Press, New York, 1977), pp. 307–323.
10. L. Ming and M. H. Manghnani, *J. Geophys. Res.* **84**, 4777 (1979).
11. R. W. G. Wyckoff, *Crystal Structures* (Interscience, New York, ed. 2, 1963), vol. 1, pp. 239–444.
12. J. C. Jamieson and B. Olinger, *Science* **161**, 893 (1968).
13. J. F. Mammone, S. K. Sharma, M. Nicol, *Solid State Commun.* **34**, 799 (1980).
14. M. Akaogi *et al.*, in *Program and Abstracts of Papers of 30th High-Pressure Conference of Japan*, Y. Syono, Ed. (Sendai, Japan, 1989), pp. 166–167 (in Japanese).
15. See, for example, K. Kusaba, M. Kikuchi, K. Fukuoka, Y. Syono, *Phys. Chem. Miner.* **15**, 238 (1988).
16. *Powder Diffraction File* (JCPDS International Center for Diffraction Data, Swarthmore, PA), Inorganic 13-307 and 24-1165.

28 August 1990; 12 December 1990

Endothelial Expression of a Mononuclear Leukocyte Adhesion Molecule During Atherogenesis

MYRON I. CYBULSKY* AND MICHAEL A. GIMBRONE, JR.

An inducible rabbit endothelial adhesion molecule that is selective for mononuclear leukocytes has been identified. This adhesion protein was expressed on the surface of activated cultured endothelium in two forms, 118 and 98 kilodaltons, the amino-terminal sequence of each being highly homologous to human VCAM-1. In dietary hypercholesterolemic and Watanabe heritable hyperlipidemic rabbit models of atherosclerosis, this adhesion molecule was found to be expressed in a localized fashion by aortic endothelium that overlies early foam cell lesions. This lesion-localized expression suggests a potential endothelium-dependent mechanism for mononuclear leukocyte recruitment during atherogenesis and may provide a molecular marker for early atherosclerosis.

THE PATHOGENESIS OF AN ATHEROSCLEROTIC plaque is a complex and chronic process that involves the focal accumulation of lipid, leukocytes, smooth muscle cells, and extracellular matrix in the intima of large arteries. Adherence of circulating monocytes and lymphocytes to the arterial endothelial lining is one of the earliest detectable events in human and experimental atherosclerosis (*1*). The subsequent transendothelial migration of these adherent leukocytes, their accumulation in the intima, transformation of monocytes into lipid-engorged "foam cells," and secretion of cytokines and growth factors are important events in the initiation and progression of atherosclerotic plaques (*1*). As atherosclerotic plaques increase in size, mononuclear leukocyte recruitment continues to be evident, predominantly at the plaque borders (*1, 2*). The localized nature and mononuclear leukocyte specificity of these cellular interactions may, in part, be a consequence of changes in the adhesive properties of the endothelial surface that involve the expression of "ATHERO-ELAMs" (inducible endothelial-leukocyte adhesion molecules that are expressed in atherosclerotic plaques). With the use of an in vitro cell culture model and a monoclonal antibody (MAb) strategy, we have now identified, immunochemically characterized, and purified a protein from lipopolysaccharide (LPS)-activated rabbit endothelial cells (ECs) that functions as a mononuclear leukocyte–selective adhesion molecule. The localization of this molecule in developing atherosclerotic lesions suggests a potential pathogenic role.

We searched for ATHERO-ELAMs in the rabbit because dietary and heritable models of atherosclerosis are well described in this animal (*3*). We established EC cultures from the aorta and inferior vena cava of normal New Zealand White rabbits (*4*) in order to study leukocyte-EC interactions. Treatment of ECs with bacterial endotoxin (LPS) induced a protein synthesis–requiring hyperadhesive surface change, which was quantitated (*5*) with cells of the U937 human myelomonocytic line (*6*) (Fig. 1, A and B). MAbs were generated to LPS-activated ECs (*7*), and we selected three of these antibodies—which are designated Rb1/9,

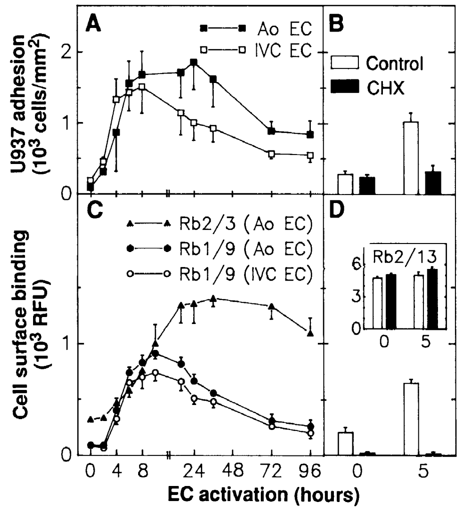

Fig. 1. U937 cell adhesion (**A** and **B**) and specific MAb binding (**C** and **D**) to EC monolayers (passage 2) derived from the aorta (Ao) and inferior vena cava (IVC) of the same New Zealand White rabbit. Activation of ECs with LPS (*Escherichia coli*; 1 μg/ml) increased both U937 cell adhesion (A) and MAb binding (C) in a time-dependent manner. The binding profile of MAb Rb1/9 was similar to the EC adhesive change for U937 cells, whereas Rb2/3 recognized a surface epitope with higher basal expression and a sustained LPS-induced expression. Rb2/4 binding was virtually identical to that of Rb1/9 (*12*). Cycloheximide (CHX) (10 μg/ml) abolished the LPS-induced increase in U937 cell adhesion (B) and Rb1/9 cell surface binding (D) during a 5-hour incubation of IVC ECs with LPS. CHX did not affect either the integrity of EC monolayers or the binding of MAb Rb2/13 (specific for an abundant constitutive EC antigen) (D, inset). In each case, data points represent the mean ± SD of quadruplicate measurements.

Vascular Research Division, Departments of Pathology, Brigham and Women's Hospital and Harvard Medical School, Boston, MA 02115.

*To whom correspondence should be addressed.